UNIVERSIDADE ESTADUAL PAULISTA
"JÚLIO DE MESQUITA FILHO"
Câmpus de São José do Rio Preto

Fabíola Costa Paciência

# Micrometric $Co_3O_4$ coated with metal-organic framework ZIF-67 for selective detection of volatile organic compounds

São José do Rio Preto

2024

Fabíola Costa Paciencia

# Micrometric $Co_3O_4$ coated with metal-organic framework ZIF-67 for selective detection of volatile organic compounds

Dissertação apresentada como parte dos requisitos para obtenção do título de Mestre em Nome do Programa, junto ao Programa de Pós-Graduação em Nome do Programa, do Instituto de Biociências, Letras e Ciências Exatas da Universidade Estadual Paulista “Júlio de Mesquita Filho”, Câmpus de São José do Rio Preto.

Financiadora: CAPES

Orientador: Profª. Drª. Diogo Paschoalini Volanti

São José do Rio Preto

2024

## IMPACTO SOCIAL DA DISSERTAÇÃO

O trabalho tem como impacto social a utilização de sensores de gás para detectar seletivamente compostos orgânicos voláteis, possibilitando o desenvolvimento de instrumentos alternativos para monitoramento da qualidade do ar e para a detecção desses compostos. Além disso, o material sintetizado é produzido de maneira simples, econômica, atóxica e sustentável.

## DISSERTATION SOCIAL IMPACT

The work has the social impact of using gas sensors to selectively detect volatile organic compounds, making it possible to develop alternative instruments for monitoring air quality and detecting these compounds. In addition, the synthesized material is produced in a simple, economical, non-toxic and sustainable way.

P117m

Paciencia, Fabiola Costa
Micrometric Co3O4 coated with metal-organic framework ZIF-67 for selective detection of volatile organic compounds / Fabiola Costa Paciencia. -- São José do Rio Preto, 2024
46 p. : tabs., fotos

Dissertação (mestrado) - Universidade Estadual Paulista (UNESP), Instituto de Biociências Letras e Ciências Exatas, São José do Rio Preto
Orientador: Diogo Paschoalini Volanti

1. Semiconductors. 2. Metal-organic framework. 3. Cobalt oxide. 4. Sensors. 5. Volatile organic compounds.. I. Título.

Sistema de geração automática de fichas catalográficas da Unesp. Dados fornecidos pelo autor(a).

**FABIOLA COSTA PACIENCIA**

# Micrometric $Co_3O_4$ coated with metal-organic framework ZIF-67 for selective detection of volatile organic compounds

Dissertação apresentada como parte dos requisitos para obtenção do título de Mestre em Química, junto ao Programa de Pós-graduação em Química, do Instituto de Biociências, Letras e Ciências Exatas da Universidade Estadual Paulista "Júlio de Mesquita Filho", Campus São José do Rio Preto.

Área de Concentração: Química

Data da defesa: 06/12/2024

Banca Examinadora:

Prof. Dr. Diogo Paschoalini Volanti

UNESP – Câmpus de São José do Rio Preto

Prof. Dr. Thiago Burgo

UNESP – Câmpus de São José do Rio Preto

Prof. Dr. Antonio Carlos Roveda Junior

USP – Instituto de Química de São Carlos

São José do Rio Preto

2024

## ACKNOWLEDGEMENTS

First, I thank God for the gift of life, for my health and for the opportunities that have allowed me to get this far. It was His constant presence, in moments of joy and challenge, that gave me the strength to persevere and achieve this goal. All honour and glory be to Him.

I would like to thank my parents, Dinah and José, who taught me to value knowledge and to never give up on my dreams, even in the face of the greatest adversity. I would also like to thank my entire family for their support and for their patience, affection and love throughout my journey.

To my sister Giovana, who has been and will always be my greatest inspiration. Her advice and trust in me have been essential to my progress. Thank you for being my greatest encourager, for believing in my potential even when I doubted it, and for always being by my side, celebrating my successes and comforting me in my difficulties.

This work is as much mine as it is yours. I thank you for everything from the bottom of my heart.

To my laboratory colleagues, especially Reinaldo and Gustavo, for their teaching and all their help in developing this research. I would like to thank my supervisor, Diogo Volanti, for the opportunity to join LabMatSus and for his guidance and support throughout this research.

I would like to thank IBILCE for all the opportunities, from undergraduate to postgraduate studies. I would also like to thank the laboratories LSQA/IBILCE-UNESP for providing the XRD and FTIR techniques, LCE DEMa/UFSCar for the TEM analysis, LMA/IQ-UNESP for SEM and EDX, and LNLS – SIRIUS for the XAS analyzes (proposal – 20232482).

This study was financed in part by the Coordenação de Aperfeiçoamento de Pessoal de Nível Superior - Brasil (CAPES) – Finance Code 001.

## RESUMO

O objetivo desse trabalho foi sintetizar o óxido de cobalto (II) dicobalto (III) ($Co_3O_4$) puro, juntamente com a síntese de $Co_3O_4$/ZIF-67, para a detecção de moléculas orgânicas voláteis. O estudo foi composto pela avaliação do uso do óxido de cobalto puro como sensor de gás em comparação com o sensor produzido a partir do óxido revestido com nanopartículas de ZIF-67 ($Co_3O_4$/ZIF-67), a fim de aprimorar a resposta, bem como a seletividade e o tempo de resposta para a detecção de VOCs. O sensor de $Co_3O_4$ foi preparado empregando o método hidrotérmico assistido por micro-ondas, ao passo que o $Co_3O_4$/ZIF-67 foi obtido utilizando o método de refluxo, utilizando o óxido puro preparado inicialmente e o ligante orgânico 2-metilimidazol. Os resultados de caracterização desses materiais demonstraram que as amostras não apresentaram impurezas. As respostas dos sensores foram avaliadas na faixa de 100 partes por milhão (100 ppm) dos VOCs: metanol, acetona, 2-butanona, m-xileno, tolueno e benzeno, variando a temperatura de operação na faixa de 200- 275°C. A maior resposta para o sensor $Co_3O_4$ foi de 20,05 para tolueno a 250 °C, ao passo que para o sensor $Co_3O_4$/ZIF-67 a maior resposta foi de 61,22 para o tolueno a 250 °C.



**Palavras-chave da dissertação:** Semicondutores. Sensor de gás. Óxido de cobalto. ZIF-67. Síntese hidrotérmica assistida por micro-ondas.

## ABSTRACT

The aim of this work was to synthesize pure cobalt (II) dicobalt (III) oxide ($Co_3O_4$), together with the synthesis of $Co_3O_4$/ZIF-67, for the detection of volatile organic molecules. The study consisted of evaluating the use of pure cobalt oxide as a gas sensor in comparison with the sensor prepared from the oxide coated with ZIF-67 nanoparticles ($Co_3O_4$/ZIF-67) in order to improve the response, selectivity and response time for the detection of VOCs. The $Co_3O_4$ sensor was prepared by the microwave-assisted hydrothermal method, while $Co_3O_4$/ZIF-67 was obtained by the reflux method using the initially prepared pure oxide and the organic 2-methylimidazole ligand. The characterizations results of these materials showed that the samples were free from impurities. The sensor responses were evaluated in the range of 100 parts per million (100 ppm) of the VOCs: methanol, acetone, 2-butanone, m-xylene, toluene and benzene, varying the operating temperature in the range of 200-275°C. The highest response for the $Co_3O_4$ sensor was 20.05 for toluene at 250°C, while the highest response for the $Co_3O_4$/ZIF-67 sensor was 61.22 for toluene at 250°C.



**Dissertation Keywords:** Semiconductors. Gas sensor. Cobalt oxide. ZIF-67. Hydrothermal synthesis.

# LIST OF FIGURES

## LIST OF TABLES

## ABREVIATIONS AND ACRONYMS LIST

| | |
|---|---|
| **BET** | Brunauer-Emmett-Teller |
| **EDX** | Energy-dispersive X-ray |
| **FESEM** | Field emission scanning electron microscopy |
| **FTIR** | Fourier transform infrared spectroscopy |
| **TEM** | Transmission electron microscopy |
| **MOF** | Metal-organic framework |
| **VOC** | Volatile organic compound |
| **RH** | Relative humidity |
| **SMO** | Semiconducting metal oxide |
| **TEY** | Total eléctron-yield |
| **XAS** | X-ray absorption spectroscopy |
| **XRD** | X-ray Diffraction |

## SYMBOLS LIST

| | |
|---|---|
| **°C** | Celsius degree |
| **cm** | Centimeter |
| **µm** | Micrometer |
| **$cm^3$ /g** | Cubic centimetre per gram |
| **eV** | Electron volt |
| **g** | Gram |
| **h** | Hour |
| **keV** | Kilo eléctron volt |
| **kV** | Kilovolt |
| **mg** | Milligram |
| **mL** | Milliliter |
| **min** | Minute |
| **ppm** | Parts per million |
| **s** | Second |
| **$m^2$ $g^{-1}$** | Square meter per gram |

# SUMMARY

# 1 INTRODUCTION AND BIBLIOGRAPHIC REVIEW

Volatile organic compounds (VOCs) represent a significant environmental concern due to their adverse effects on human health and the natural environment (LI et al., 2021). These compounds are recognized as toxic and are linked to the development of allergic reactions. It is therefore of great importance to be able to detect gaseous pollutants, such as volatile organic compounds, in a number of different fields, including the pharmaceutical industry, the food industry, environmental monitoring and public safety. In light of these developments, it is important to acknowledge the emergence of gas sensors as a tool for the detection of environmental contaminants, including gases and volatile organic compounds. Considering the multitude of gas detection technologies that have emerged in recent years, it is imperative to underscore the growing prominence of metal oxide semiconductors (MOSs) and their nano composites for the detection of gases and volatile organic compounds. This is largely due to their high porosity, which enhances their gas detection capacity, and their heightened sensitivity (WANG et al., 2023).

Metal oxide semiconductor gas sensors have broad application prospects in various fields due to their characteristics of small size, low cost, fast response speed, and real-time in situ detection (HU et al., 2024). However, the field of gas sensors has developed mainly based on *n*-type semiconductors, with little research and application of the detection properties of *p*-type oxide semiconductors. (LIU; ZHANG; WU, 2011) This is due to the high sensitivity and short response range of n-type semiconductors, which is advantageous for a significant proportion of research. However, due to their elevated operating temperature, they are not suitable for practical applications. While *p*-type semiconductors exhibit excellent stability and a low operating temperature range, they display reduced sensitivity (YAO et al., 2022). Among the *p*-type MOS, $Co_3O_4$ is a multifunctional semiconductor that exhibits sensitivity to gas detection due to the fact that the $Co^{2+}$ present in the oxide can be readily oxidized to a higher oxidation state, thereby facilitating the adsorption of oxygen molecules on the material's surface, which is advantageous for gas detection (HU et al., 2024).

Moreover, a gas sensor's capacity to selectively VOCs is of paramount importance. Additionally, the ability to detect gases at exceedingly low concentrations (ranging from ppb to ppm) in mixtures devoid of interference from other substances is a crucial attribute. (VAN DEN BROEK et al., 2021). Despite the efficacy of p-type semiconductors as VOC catalysts, the issue of low detection sensitivity persists, a challenge that is particularly prevalent in cobalt oxides. To enhance the sensitivity of the sensor, modifications are essential.

It bears noting that recent studies have explored the potential of metal-organic frameworks (MOFs) as filtration materials to enhance the detection of MOSs. This improvement is often attributed to a size-screening effect (LUO et al., 2023). By leveraging this effect, it is possible to modify and adjust the pore size to achieve greater selectivity for specific gases, taking into account both the diameter of the MOF utilized and the gas under analysis. Therefore, the utilization of filters is intended to enhance the selectivity of the sensor, as they transform undesired interferents into inactive or less responsive substances, while the target analytes remain ideally unaffected. However, the utilization of filters can also enhance the sensitivity of the sensor by rendering certain analytes more responsive (WEBER; GÜNTNER, 2022).

## 1.1 Detection of volatile organic compounds

Volatile organic compounds are a class of organic substances that can be produced by both natural and synthetic processes. They are one of the primary classes of pollutants, both internally and externally. The World Health Organization (WHO) has identified a number of adverse effects of VOCs on human health, including the triggering of various chronic and acute diseases. Additionally, these compounds have been linked to destructive effects on the central nervous system (CNS), (HAJIVAND et al., 2024). Furthermore, VOCs have been shown to have a detrimental impact on the environment. In light of these considerations, it is evident that the detection of volatile organic compounds is a crucial endeavor in contemporary research.

Sensitive analytical techniques have been developed and employed for the quantification of VOCs, including spectrophotometry, gas chromatography (GC), and high-performance liquid chromatography (HPLC) (MIRZAEI; LEONARDI; NERI, 2016). However, despite their accuracy, these techniques have some disadvantages,

including high cost, high energy demand, low yield, and the necessity for complex pre-treatment steps, which renders them unsuitable for scenarios where VOC monitoring is required rapidly and at a low cost. Consequently, research has been conducted over time with the aim of developing high-performance, user-friendly, and cost-effective gas detection devices that exhibit high sensitivity, selectivity, and stability for specific applications. These studies have resulted in the development of a diverse array of sensors based on MOFs, microporous materials whose surface functionality can be tailored to provide stronger and more selective binding sites for the targeted adsorption of VOC molecules through suitable coordination bonds or based on electrostatic interactions. These sensors demonstrate superior potential for detection when compared to other types of sensors, due to their high responsiveness and ease of integration.

Metal-organic frameworks are microporous materials whose surface functionality can be adapted to provide stronger and more selective binding sites for targeted adsorption of volatile organic compounds through suitable coordination bonds or electrostatic interactions. This adaptability confers superior potential for detection when compared to other types of sensors, due to their high responsiveness and ease of integration.

## 1.2. Semiconductors metal oxides of $Co_3O_4$ for VOC detection

Metal oxide semiconductors are a prominent emerging technology in the field of gas detection. Derived from MOFs, MOSs possess high porosity, which enhances their capacity for gas detection. In comparison to alternative detection methodologies, these sensors demonstrate enhanced sensitivity and stability, reduced manufacturing costs, straightforward applicability, and a diverse range of structures and morphologies (WANG et al., 2023).

In this regard, among the various sensors derived from semiconducting metal oxides, $Co_3O_4$ is a notable transition metal oxide. Its status as a p-type semiconductor material has led to extensive research on its potential as a material for gas sensors, given its high thermal stability. Additionally, its oxygen absorption capacity (LETSHOLATHEBE et al., 2021) qualifies it as an effective gas detector, as the conversion of $Co^{2+}$ and $Co^{3+}$ between different valence states enhances the material's sensitivity to gas detection (XU; CHENG, 2016).

Moreover, research suggests that the gas detection capabilities of $Co_3O_4$ micro and nanostructures are significantly influenced by their surface area, porous structure, and morphology. As documented in the findings of numerous researchers, the synthesis of diverse nanostructures of the material, including nanowires (BAI et al., 2013), nanotubes (FEI et al., 2012; ZHONG et al., 2020) and nanorods (YAN et al., 2017), in order to enhance the material's performance. The resulting structures have demonstrated differing detection responses, suggesting that the material's performance can be tailored through structural engineering. (LI et al., 2021). Consequently, the gas detection properties of $Co_3O_4$ structures - micro and nano - are contingent upon the modification of one of the aforementioned properties (XU; CHENG, 2016).

*Therefore, the main objective of this work is to study the micrometric $Co_3O_4$ oxide morphology. This structure was selected over the manometric structure with the intention of more effectively covering the material with a metal organic framework (MOF) and enhancing the sensor's sensitivity by incorporating ZIF-67 into the material. Secondary objectives include: (a) A comparison of selectivity in the presence and absence of ZIF-67; (b) An examination of the application of a VOC sensor at different working temperatures (in different operating conditions, such as relative humidity (RH) and atmospheric working temperature; and (c) the synthesis of a material capable of detecting VOCs at low concentrations (ppm) with high selectivity, fast response time, low recovery time, stability and reversibility.*

# 2 Micrometric $Co_3O_4$/ZIF-67 with high toluene detection capability

**ABSTRACT**

The detection of volatile organic compounds (VOCs), particularly toluene, has become a crucial aspect of environmental monitoring due to the pervasive use of these compounds and their associated risks to human health and the environment. In this study, we present the synthesis of micrometer-sized $Co_3O_4$, a p-type semiconductor, using a microwave-assisted hydrothermal method followed by calcination. Given the inherent low sensitivity and selectivity of p-type metal oxide semiconductor (MOS) sensors, we explored strategies to enhance the selectivity and sensitivity of p-type MOS under diverse sensing conditions, including varying temperatures and humid environments. The VOC detection performance of $Co_3O_4$ was improved by adding a metal-organic framework, ZIF-67. The $Co_3O_4$/ZIF-67 composite was prepared using the reflux method. The sensor demonstrated enhanced detection capabilities compared to pure $Co_3O_4$, as evidenced by the $Co_3O_4$/ZIF-67 composite exhibiting the highest response (61.22) to 100 ppm toluene at 250 °C, with a high selectivity index (5.43). In contrast, the $Co_3O_4$ sensor responded 20.05 to toluene, with a relatively low selectivity index (2.86) at 250 °C. Therefore, the incorporation of ZIF-67 resulted in an enhancement of the sensor's response and selectivity. Furthermore, the sensor demonstrated satisfactory performance at various controlled relative humidities. These findings highlight the potential of micro-sized $Co_3O_4$/ZIF-67 as a promising candidate for low-temperature toluene sensing, which is critical for environmental and human health monitoring purposes.

**Keywords**: *p*-type semiconductors, ZIF-67, cobalt oxide, gas sensor, toluene

## 2.1 Introduction

The monitoring and detecting of gases that are harmful to the environment and human health is a constant concern, particularly about volatile organic compounds (VOCs) (LEIDINGER et al., 2014), due to the potential risks to human health and the environment. In addition to their use as solvents in various industrial processes, VOCs are employed in household products, rendering them indoor and outdoor pollutants (MOLHAVE, 1991). Among the different classes of VOCs, toluene, a typical aromatic compound, is widely used in many industrial activities (WANG et al., 2025) and is one of the most prevalent atmospheric pollutants, contributing significantly to global climate change (CHEN et al., 2024). Furthermore, a growing body of evidence indicates that exposure to toluene may have adverse effects on several organ systems, including the skin, kidneys, liver, and central nervous system (PERRONE et al., 2023). Additionally, a substantial body of scientific literature indicates that toluene is a carcinogen (WANG et al., 2025). It highlights the importance of developing and implementing sensitive and cost-effective techniques for detecting toluene gas, particularly for immediate surveillance, which is essential for protecting human health and the environment.

The search for effective VOC monitoring methods is intensifying to establish air quality control and monitoring tools (MIRZAEI; LEONARDI; NERI, 2016). Gas chromatography (VESELY et al., 2003) and high-performance liquid chromatography (SABOURIN; BECHTOLD; HENDERSON, 1988) are two susceptible analytical techniques used to quantify VOCs precisely. However, despite these techniques' high precision and accuracy, they possess certain disadvantages, including high cost, high energy demand, and low yield. Furthermore, these techniques necessitate time-consuming and intricate preliminary processing and highly trained operators' expertise (MIRZAEI; LEONARDI; NERI, 2016). In contrast, gas sensors based on semiconductor metal oxide (SMO) represent an optimal solution for detecting VOCs in both industrial and domestic settings. These sensors offer a compact design, low production costs, and real-time monitoring (THEODORO et al., 2023; ZITO et al., 2024), making them highly suitable for various applications.

SMO possesses the advantageous characteristics of a high detection response and excellent operational stability, making this material a ubiquitous tool for detecting many gases. Recent studies have indicated that *p*-type SMO gas sensors,

including those based on NiO (CHEN et al., 2019), CuO (MARIAMMAL; RAMACHANDRAN, 2018), $Cr_2O_3$ (XIE et al., 2024), and $Co_3O_4$ (QUANG et al., 2018), have the potential to detect toxic toluene gas effectively (WANG et al., 2022). Wang et al. prepared $Co_3O_4$ NWs gas sensors using the rigid mold method, which demonstrated a high level of responsiveness to toluene gas (WANG et al., 2021). Liu et al. prepared a toluene gas sensor from hollow NiO/ZnO microspheres, which exhibited a response value of 240 for 100 ppm toluene at 300 °C (LIU et al., 2022). *P*-type sensors are primarily utilized due to their favorable thermal stability, their propensity for facile oxygen exchange between the network and the surrounding air, and the multiple stable oxidation states and the high concentrations of positive holes present in this type of material, which are indispensable for the advancement of high-performance VOC sensors (CHO et al., 2016). Unfortunately, p-type sensors do not perform well in their original form due to low selectivity (BAGHERZADEH ENFERADI; MIRZAEI, 2024). To improve their gas detection performance, it is common practice to combine them with metal ions, carbon compounds, or noble metals(SAAD et al., 2024). An additional avenue for exploration is introducing a metal-organic framework into the sensor material structure, such as ZIF-67. However, it should be noted that, to the best of our knowledge, there is a lack of research in the literature on $Co_3O_4$/ZIF-67 composite microstructures for the detection of volatile organic compounds (VOCs), particularly toluene. Alternatively, studies have been conducted on composites utilizing ZIF-67 to detect specific VOCs. For instance, Malepe et al. developed a sensor comprising carbon soot and ZIF-67, demonstrating high sensitivity and selectivity for acetone detection under ambient temperature conditions (MALEPE et al., 2023).

This study details the enhancement of the VOC detection properties of $Co_3O_4$ by introducing the metal-organic framework ZIF-67, resulting in the formation of a $Co_3O_4$/ZIF-67 composite via the reflux method. The sensor measurements demonstrated that the composite responded to toluene in controlled dry and humid atmospheres, outperforming the pure $Co_3O_4$ sample. Furthermore, the $Co_3O_4$/ZIF-67 composite exhibited approximately twice the selectivity of the $Co_3O_4$ sample, indicating that the incorporation of ZIF-67 enhanced the selectivity of the material.

## 2.2 Methods

### 2.2.1 Chemicals and materials

This study utilized high-purity materials (greater than 99%) sourced from Sigma-Aldrich, including cobalt nitrate hexahydrate $Co(NO_3)_2{\cdot}6H_2O$, ammonium fluoride ($NH_4F$), urea ($CH_4N_2O$), 2-methylimidazole, and dimethylformamide (DMF). Deionized (DI) water was purified using a Milli-Q system (18.2 MΩ $cm^{-1}$ at 25 °C, Millipore) for the synthesis process. The VOCs in detection measurements also comprised high-purity reagents (≥ 99%), including methanol, acetone, 2-butanone, m-xylene, toluene, and benzene.

### 2.2.2 Synthesis of pure $Co_3O_4$ and $Co_3O_4$/ZIF-67

The initial phase of the process entails the synthesis of $Co_3O_4$, which is based on a modification of a previously reported procedure (LI et al., 2021). Initially, 1.20 g of cobalt nitrate hexahydrate were dissolved in 80.0 milliliters of deionized water. Subsequently, 0.30 g of $NH_4F$ and 1.50 g of urea were added, and the resulting solution was stirred for 30 minutes and transferred to an apparatus comprising a polytetrafluoroethylene autoclave sealed with a stainless-steel frame and heated to 150 °C for 90 minutes in a microwave (2,45 GHz/800W) (E.L. DA SILVA et al., 2010). Once cooled to room temperature, the pink solid was centrifuged (8.000 rpm) and washed with deionized water and ethanol. The resulting precipitate was then dried at 80 °C for approximately 12 h. Finally, $Co_3O_4$ was obtained by calcination at 300 °C for 2 h with a heating rate of 2 ° C/min. The procedure for synthesizing $Co_3O_4$/ZIF-67 was adapted from previous methods described in the literature (CAI et al., 2017). The reflux method was employed to combine 0.098 g of previously synthesized $Co_3O_4$ with 0.27 g of the ligand (2-methylimidazole), 25.0 mL of DMF, and 8.0 mL of deionized water. Subsequently, the solution was stirred under reflux for 20 h at 70°C. The resulting solid was washed with ethanol and dried in an oven at 80 °C for 12 h.

### 2.2.3 Characterizations

The phase composition of the samples, $Co_3O_4$ and $Co_3O_4$/ZIF-67, was characterized by X-ray diffraction (XRD) collected in a Rigaku MiniFlex 300 powder

diffractometer, utilizing Cu Kα radiation (λ =1.5418 Å), operated at 30 kV and 10 mA. Measurements were conducted over a range of 5-80° in 2θ, with a step size of 0.01° and a scan rate of 1° $min^{-1}$. Fourier transform infrared spectroscopy (FTIR)was conducted with a Perkin Elmer Spectrum Two spectrophotometer, operated in the 400-4000 $cm^{-1}$ region without a heating process. The microstructure was observed using a JEOL JSM-6701F field emission scanning electron microscope (FESEM), operated at an accelerating voltage of 2 kV to understand the morphology observed in the samples. A chemical mapping analysis of the corresponding elements was conducted using energy-dispersive X-ray (EDX). Additionally, transmission electron microscopy (TEM), high-resolution electron microscopy (HRTEM), and selected area electron diffraction (SAED) were performed using a microscope, JEM 2100 F (JEOL), operated at 200 kV. The total electron yield and fluorescence yield signals were measured by X-ray absorption spectroscopy (XAS), which was conducted at the IPE (Inelastic scattering and PhotoElectron spectroscopy) beamline at the synchrotron light source (SIRIUS), which is located at the LNLS. The surface area was verified using a Micromeritics Gemini VII (model 2390 t) via the Brunauer-Emmett-Teller (BET) method.

### 2.2.4 Sensor measurements and VOC fabrication

To prepare the sensors, 0.5 mg of $Co_3O_4$ and 0.3 mg of $Co_3O_4$/ZIF-67 were dispersed in 0.5 mL of isopropanol under an ultrasonic bath (frequency of 50/60 Hz and 280 W) for 10 min. Subsequently, 30 µL of the dispersion was deposited onto an alumina substrate containing interdigitated Au electrodes (10.0 mm x 8 mm) with a distance of 0.1 mm between the gold trills, followed by a heating period of 10 min at a temperature of 200 °C. Subsequently, the sensor was placed within a tube furnace, which was equipped with a gas inlet and outlet, and monitored by a thermocouple that was inserted under a synthetic pure air atmosphere with a flow rate of 250 mL $min^{-1}$, connected to a Keithley SourceMeter 2400 high-voltage measurement unit with an applied voltage of 5 and 1 V, as shown in Fig. 1.

**Fig. 1.** Schematic of the sensor measurement system

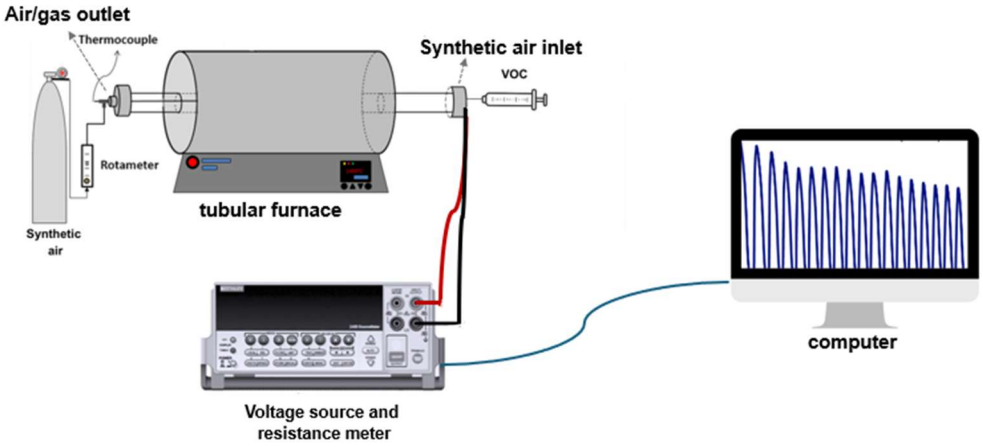


Source: Author

Measurements were conducted at varying operational temperatures within the range of 200 to 275 °C and the change in material resistivity was also studied under varying environmental conditions, including relatives humidities. The selected VOCs, including methanol (M), acetone (A), 2-butanone (2B), m-xylene (MX), toluene (T), and benzene (B), were prepared in separate vials and introduced individually into the gas chamber with a syringe. To establish relative humidity (RH) levels of 60 % and 80%, saturated saline solutions of NaCl and $K_2SO_4$ were used, respectively, with monitoring provided by a portable HANNA thermohygrometer (model HI 9564). The responses for the selected VOCs were determined using the $R_{VOC}/R_{air}$ ratio. $R_{VOC}$ and $R_{air}$ represent the material's resistance after contact with the VOC and the material's resistance in clean air, respectively.

## 2.3 Results and discussion

### 2.3.1 Materials characterization

The XRD patterns of the synthesized samples are shown in Fig. 2a. The diffraction peaks at 19.0, 31.3, 36.9, 44.8, 59.4, 65.2, and 77.3° correspond to the (111), (220), (311), (222), (400), (422), (511) and (400) planes, which are in excellent agreement with the standard XRD data for $Co_3O_4$ in the cubic phase (PDF #74-2120), indicating that the desired phase has been obtained. The absence of additional peaks proves that pure oxide has been obtained. As shown in Fig. 2a, the XRD pattern for the $Co_3O_4$/ZIF-67 compound showed the absence of the characteristic ZIF-67 peaks

at 7.4, 10.4, 12.8, and 17.9° (DONG; ZHANG; MA, 2023), with only the peaks related to the previously mentioned planes of the cobalt oxide being observed. Therefore, the crystallinity of $Co_3O_4$ was not altered by the introduction of ZIF-67.

The functional groups in the materials were investigated using FTIR analysis. The spectra of $Co_3O_4$ and $Co_3O_4$/ZIF-67 are shown in Fig. 2b, where similar profiles were observed. The highest intensity peaks at 547 and 654 $cm^{-1}$, which originate from the stretching vibrations of the Co-O bonds, confirm the formation of the cobalt oxide spinel since $Co_3O_4$ consists of a mixture of the two oxidation states of cobalt, in which $Co^{3+}$ occupies octahedral sites and $Co^{2+}$ tetrahedral sites within the crystal lattice (XU; CHENG, 2016). Thus, the 547 $cm^{-1}$ band is characteristic of the $Co^{3+}$- O vibration in the octahedral site, and the 654 $cm^{-1}$ band is attributed to the $Co^{2+}$- O vibration in the tetrahedral site. The less intense band of around 3400 $cm^{-1}$ of $Co_3O_4$ is due to the O-H stretching vibrational mode of the adsorbed water molecules, and the absence of a band corresponding to nitrate ions indicates complete removal by the synthesis method used (MAKHLOUF et al., 2013). As observed in Fig. 2b, the FTIR spectra for the $Co_3O_4$/ZIF-67 compound showed the absence of the characteristic bands of ZIF-67 at 1423 cm and 1306 $cm^{-1}$, corresponding to the stretching vibrations of the imidazole ring of ZIF-67. The peak at 945 $cm^{-1}$, attributed to the bending of the ring, and the peaks of the Co-N (431 $cm^{-1}$) and C=N (1578 $cm^{-1}$) bonds (DONG; ZHANG; MA, 2023), with only the peaks related to the previously mentioned characteristic bands of the cobalt oxide being observed.

**Table 1**. A comparison of the surface area, pore dimensions, and pore volume of the materials synthesized in this study.

| **Material** | **Surface area ($m^2g^{-1}$)** | **Pore size (nm)[a]** | **Pore volume ($cm^3/g$)[b]** |
|---|---|---|---|
| $Co_3O_4$ | 62.7 | 35.3 | 0.554 |
| $Co_3O_4$/ZIF-67 | 68.2 | 26.1 | 0.445 |

[a] Adsorption average pore diameter (4V/A by BET); [b] Single point adsorption total pore volume of pores less than 1952.438 Å width at p/p° = 0.990000000.

Source: Author

Fig. 2c,d shows the nitrogen adsorption and desorption isotherms for the oxide and the composite, which display significant similarities in their profiles. The details

of the material's pore size distribution and specific surface area are provided in Table 1. It is evident that the $Co_3O_4$ and $Co_3O_4$ /ZIF-67 samples have specific surface areas of 62.7 and 68.2 $m^2 g^{-1}$, respectively, and they also possess notable pore volumes of 0.554 and 0.445 $cm^3/g$, respectively.

These findings are indicative of the formation of mesoporous materials. The introduction of ZIF-67 caused an increase in the specific surface area, accompanied by a slight decrease in pore size attributed to the deposition of ZIF-67 nanoparticles beneath the pores of the $Co_3O_4$ microrods.

**Figure 2.** XRD patterns of (a) $Co_3O_4$ and $Co_3O_4$/ZIF-67. FTIR spectra of (b) $Co_3O_4$ and $Co_3O_4$/ZIF-67. Isotherms by nitrogen adsorption and desorption for $Co_3O_4$ (c) and $Co_3O_4$/ZIF-67 (d).

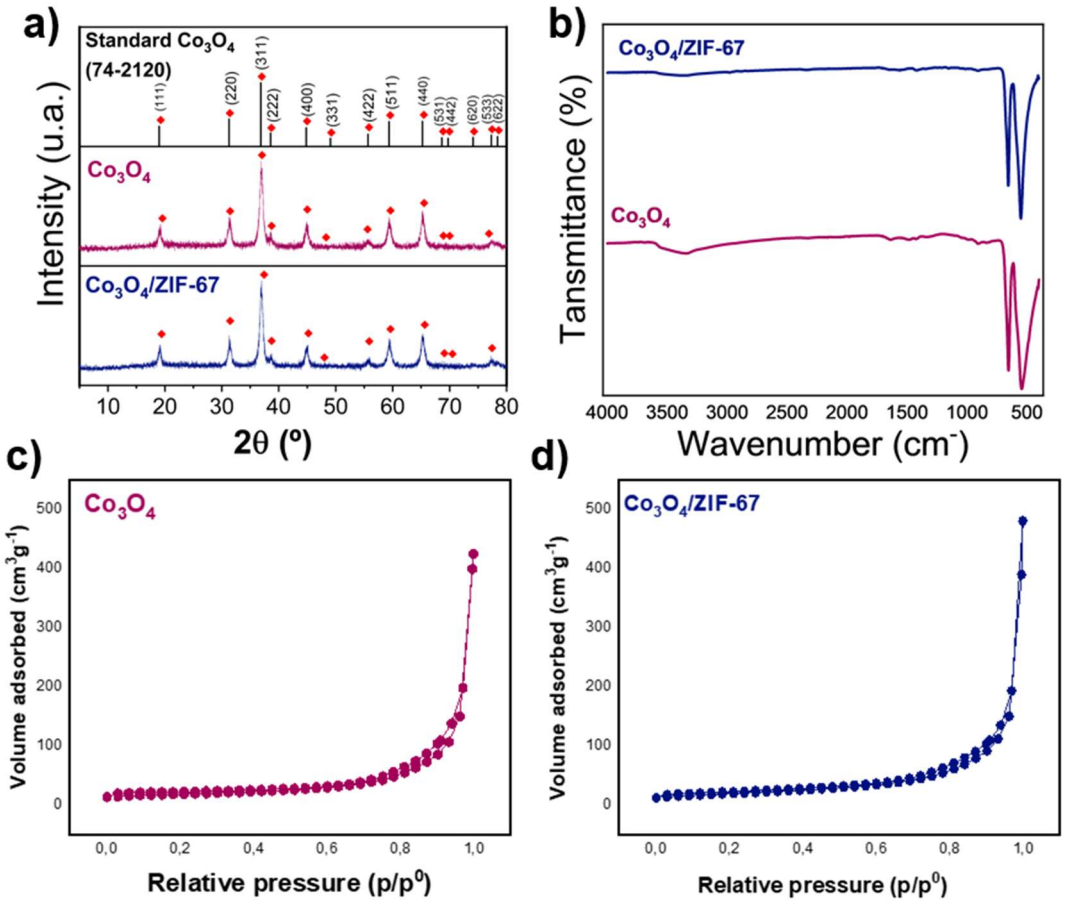


Source: Author

Fig.3a shows the $Co_3O_4$ microrods superimposed and randomly distributed, according to FESEM analysis. Fig.3b illustrates a single microrod of the cobalt oxide.

Fig.3c,d shows the $Co_3O_4$/ZIF-67 composite covered with a small amount of ZIF-67 nanoparticles on the surface, which have an irregular shape and are unevenly distributed over the material's surface. Furthermore, the results show that $Co_3O_4$/ZIF-67 retained the morphology of $Co_3O_4$ microrods. It can also be seen that the typical core-shell structure was not obtained (where the shell would consist of ZIF-67 and the core of $Co_3O_4$ so that the shell would act as a filter covering the entire material).

**Figure. 3.** FESEM images of (a) $Co_3O_4$ microrods agglomerated, (b) isolated microrod of $Co_3O_4$. And different magnifications of (c,d) $Co_3O_4$/ZIF-67.

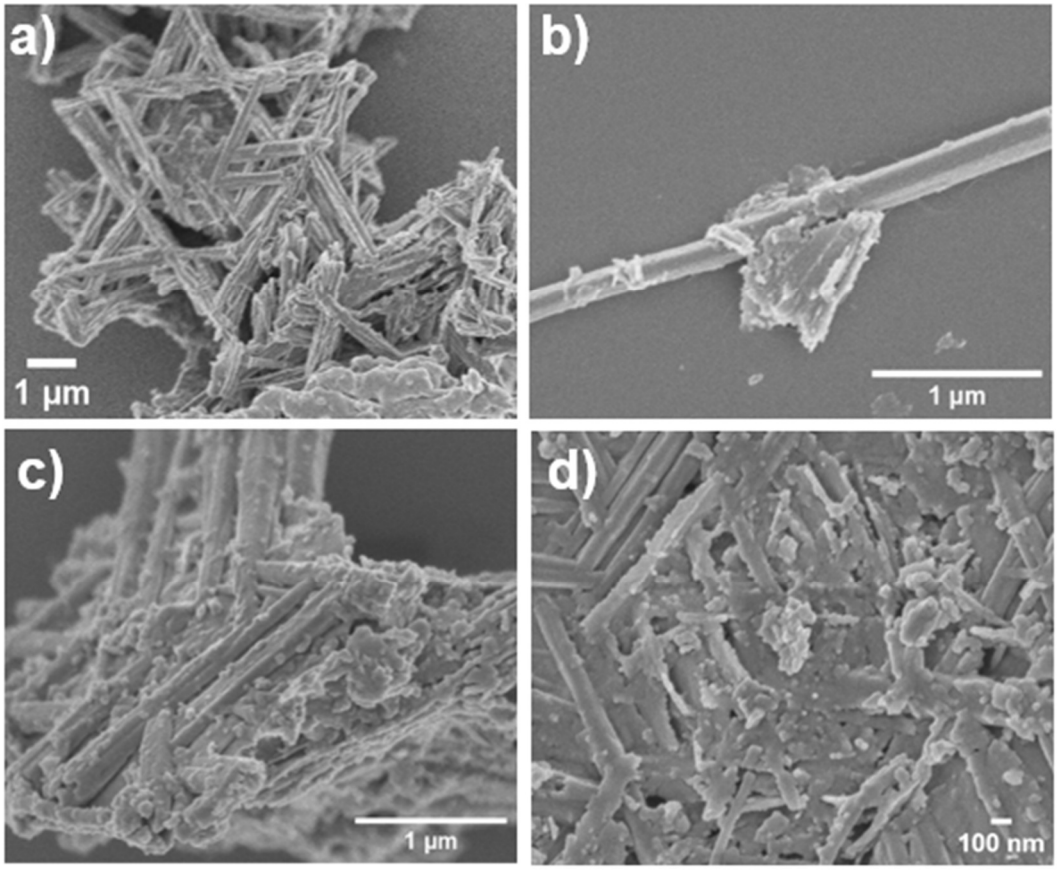


Source: Author

Transmission electron microscopy (TEM) analysis provides valuable insights into the structural and morphological characteristics of the $Co_3O_4$ and $Co_3O_4$/ZIF-67 samples. Fig.4a,e presents bright-field transmission electron microscopy (BF-TEM) images, illustrating the microrod structures of $Co_3O_4$ and $Co_3O_4$/ZIF-67, respectively. Both samples exhibit dense decoration of the $Co_3O_4$ microrods with nanoparticles. Notably, the incorporation of ZIF-67 into the $Co_3O_4$/ZIF-67 composite introduces additional nanoscale features, indicating successful hybridization of the materials.

The selected area electron diffraction (SAED) patterns in Fig.4b,f confirm the crystallinity and phase composition of the materials. Fig.4b demonstrates the indexed diffraction spots corresponding to the cubic phase of $Co_3O_4$, with planes such as (111), (220), and (311) identified, aligning with the literature. Fig.4f exhibits similar cubic $Co_3O_4$ reflections and enhanced diffraction intensity, which can be attributed to the well-distributed ZIF-67 nanoparticles.

The high-resolution TEM (HRTEM) images in Fig.4c,g reveal lattice fringes characteristic of the crystalline planes of $Co_3O_4$ and the $Co_3O_4$/ZIF-67 composite. We can confirm the presence of specific crystallographic planes by extracting the interplanar distances from these images.

A novel plane mapping technique was employed to analyze the structural features further, as depicted in Fig.4d,h. This technique utilizes the Fourier transform (FFT) of the HRTEM images to isolate spots corresponding to individual planes. By applying inverse FFT (IFFT) to each selected spot, individual plane images are reconstructed and color-coded to distinguish specific crystallographic planes. These color-coded maps are then compiled using graphic design software, ensuring a clear visualization of the spatial distribution of planes within the sample.

The mapping demonstrates the distribution of crystallographic planes in $Co_3O_4$ and $Co_3O_4$/ZIF-67. This advanced visualization underscores the composite's structural integrity and high crystallinity, which are pivotal for its gas-sensing capabilities. The findings confirm that incorporating ZIF-67 nanoparticles into $Co_3O_4$ does not disrupt the cubic structure but enhances the material’s complexity and potential functionality.

**Figure 4.** TEM characterization of $Co_3O_4$ and $Co_3O_4$/ZIF-67 samples. (a) and (e) Bright-field TEM images reveal the microrod structure of $Co_3O_4$ and $Co_3O_4$/ZIF-67, respectively. (b) and (f) Selected area electron diffraction (SAED) patterns indexed to the cubic phase of $Co_3O_4$. (c) and (g) High-resolution TEM (HRTEM) images display lattice fringes of $Co_3O_4$ and $Co_3O_4$/ZIF-67. (d) and (h) Plane maps analysis highlights the distribution of planes in $Co_3O_4$ and $Co_3O_4$/ZIF-67, showcasing their structural integrity and enhanced complexity.

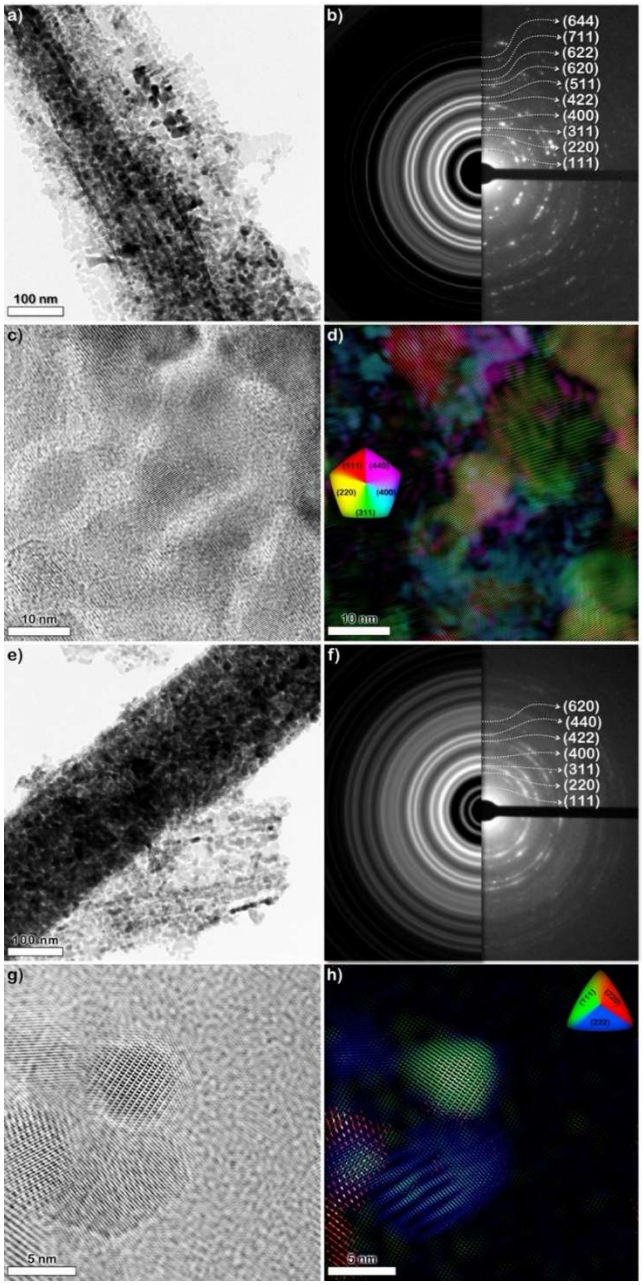


Source: Author

The EDX technique was employed to examine the distribution of elements within the samples, as illustrated in Fig. 5. The EDX spectra for $Co_3O_4$ and $Co_3O_4$/ZIF-67 are presented in Fig. 5a and Fig. 5b, respectively, and show only X-ray emission peaks for O and Co. The absence of additional emission peaks indicates the presence of impurities in both samples. The TEM images corresponding to the EDX analysis area for $Co_3O_4$ and $Co_3O_4$/ZIF-67 are depicted in Fig. 5c-d, respectively. Only O and Co were detectable in both samples, as demonstrated in Fig. 5e-h.

**Figure. 5.** EDX spectra showing the elemental analysis of (a) $Co_3O_4$ and (b) $Co_3O_4$/ZIF-67. TEM images focusing on the EDX region of (c) $Co_3O_4$ and (d) $Co_3O_4$/ZIF-67. EDX mapping images for (e-f) $Co_3O_4$ and (g-h) $Co_3O_4$/ZIF-67.

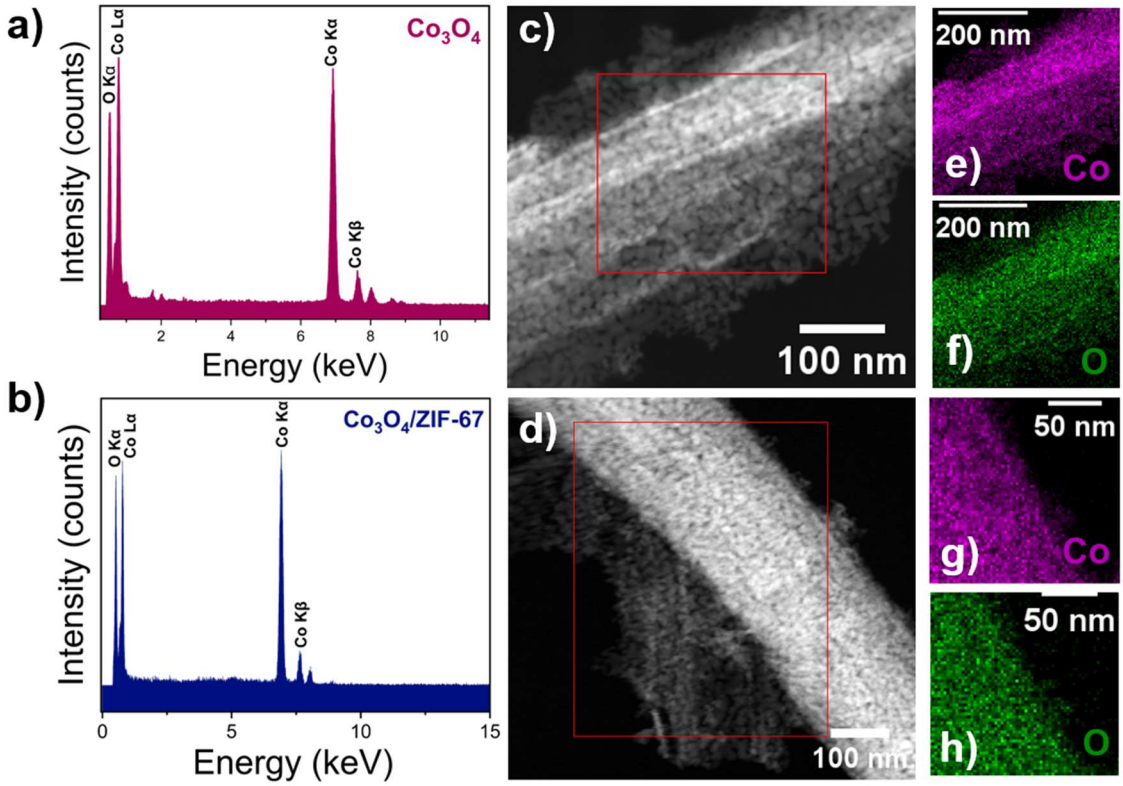


Source: Author

The total electron yield (TEY) X-ray absorption spectroscopy (XAS) method investigated the samples' valence states and atomic structures. Fig.6a depicts the $L_2$ and $L_3$ edge spectra of the Co materials, wherein the peaks observed in the 780 and 795 eV regions are attributed to $L_3$ and $L_2$, respectively. The $L_3$ edge region of Co exhibits a notable lower energy peak (1) at 779 eV and a pronounced higher energy peak (2) at 780.4 eV, which are ascribed to the $Co^{2+}$ and $Co^{3+}$ ions, respectively

(FENG et al., 2021). The L-edge of Co is divided into two peaks ($L_2$ and $L_3$) due to spin-orbital coupling at the core level. The lower energy $L_3$ peak is attributed to $2p_{3/2}$ → 3d, while the $L_2$ peak is associated with $2p_{1/2}$ → 3*d* (WANG et al., 2018). Fig.6b depicts the spectra for the O K-edge of the samples, exhibiting a peak of greater intensity (1) at 530 eV, indicative of oxygen species hybridized with low spin $Co^{3+}$ states (ZHANG et al., 2023) and a peak of lesser intensity (2) at 542.8 eV. Fig.6c depicts the XAS spectrum at the K edge of the N atom in the $Co_3O_4$/ZIF-67 sample, exhibiting two distinct peaks: one at 390.2 eV (1) and another at 397.4 eV (2). The peak at 397.4 eV can be attributed to the transition of nitrogen 1s electrons to anti ligand 2*p* orbitals hybridized with cobalt 3*d* orbitals (LOU et al., 2018). The absence of a peak near 402 eV, characteristic of the N-O bond, indicates that the nitrogen atoms are bonded exclusively to cobalt (WANG et al., 2018).

X-ray absorption spectroscopy (XAS) proved to be the most crucial characterization technique performed, as it was the only technique able to detect the presence of nitrogen in $Co_3O_4$/ZIF-67, indicating that the deposition of the ligand using the reflow technique was successful. Furthermore, the presence of nitrogen was only confirmed in the TEY investigations, suggesting that it is predominantly located in the bulk regions of the sample.

**Figure. 6.** XAS spectra in TEY mode around the (a) Co $L_{2,3}$ -edges, (b) O K-edges of the $Co_3O_4$ and $Co_3O_4$/ZIF-67, and (c) N K-edges of the $Co_3O_4$/ZIF-67.

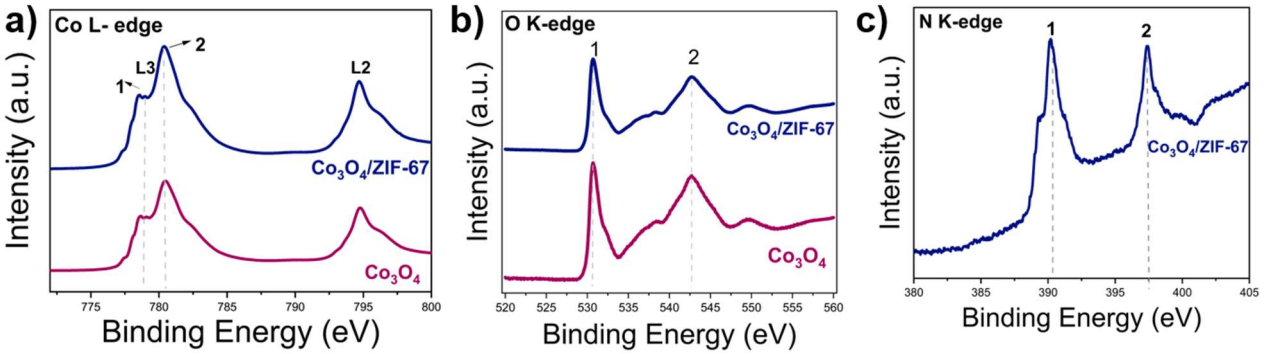


Source: Author

### 2.3.2 VOCs sensing measurements

The performance of the $Co_3O_4$ and $Co_3O_4$/ZIF-67 materials in the detection of VOCs was evaluated under a range of operational conditions, with temperatures spanning from 200 to 275 °C and dry air against six VOCs, namely methanol (M), acetone (A), 2-butanone (2B), m-xylene (MX), toluene (T) and benzene (B). No notable outcomes were observed in the temperature range below 200 °C or above 275 °C.

The selected VOCs were measured at 100 ppm to ascertain the selectivity of the sensors. Fig.7a illustrates the selectivity outcomes for the $Co_3O_4$ sensor. The results demonstrate that the sensor exhibited heightened responses at temperatures of 250 °C, with the highest response (20.0) observed for toluene detection. Fig.7b illustrates the selectivity of the $Co_3O_4$/ZIF-67 sensor. The incorporation of ZIF-67 resulted in an enhanced response for specific VOCs within the 225-250 °C range. Therefore, the sensor exhibited its most excellent response (61.2) to toluene at 250 °C. The two sensors exhibited comparable performance at temperatures exceeding 250 °C, demonstrating their optimal selectivity indices at this temperature, as illustrated in Fig.7c. The selectivity index of the sensors was determined by comparing the responses of the target gas (toluene) with those of the interfering gases. The selectivity index is the ratio between the response of a target gas and that of an interfering gas ($R_{VOC\text{-}target}$ /$R_{VOC\text{-}interfering}$ ). (YIN et al., 2020) The pure oxide exhibited a selectivity index of 2.86, whereas the second sensor demonstrated a selectivity index 5.43 at 250 °C. Furthermore, the $Co_3O_4$ sensor demonstrated inferior performance to the second sensor, as evidenced by a selectivity index approximately double that of the pure oxide sensor.

We can, therefore, conclude from these SI results that $Co_3O_4$/ZIF-67 exhibited higher detection performance than $Co_3O_4$ at 250 °C. The results can be explained by the incorporation of ZIF-67 into cobalt oxide; another justification consists of the surface area of the sensors, where $Co_3O_4$/ZIF-67 (68.2 $m^2 g^{-1}$) presented a larger surface area than Co3O4 (62.7 $m^2 g^{-1}$), a larger surface area allows for a more significant number of active sites to interact with target gas molecules, thereby increasing the selectivity of the sensor. (DEY, 2018; WANG et al., 2010)

The response time was determined by measuring 90% of the maximum resistance following the introduction of the VOC. The recovery time indicates the time

needed to return to 90% of the original baseline. These data are shown in Fig.7d-e for the $Co_3O_4$ and $Co_3O_4$/ZIF-67 samples. The $Co_3O_4$ sensor demonstrated a response time ($T_{resp}$) of 78.9 s and a recovery time ($T_{rec}$) of 241.7 s, while the other sensor showed response and recovery times of 93.2 s and 224.3 s, respectively.

**Figure. 7.** Selectivity in dry atmosphere sensor measurements from 200 to 275 °C to 100 ppm of different VOCs of (a) $Co_3O_4$ and (b) $Co_3O_4$/ZIF-67. (c) Radar graph of selectivity ratio. Response and recovery times to 100 ppm of toluene at 250 °C of (d) $Co_3O_4$ and (e) $Co_3O_4$/ZIF-67.

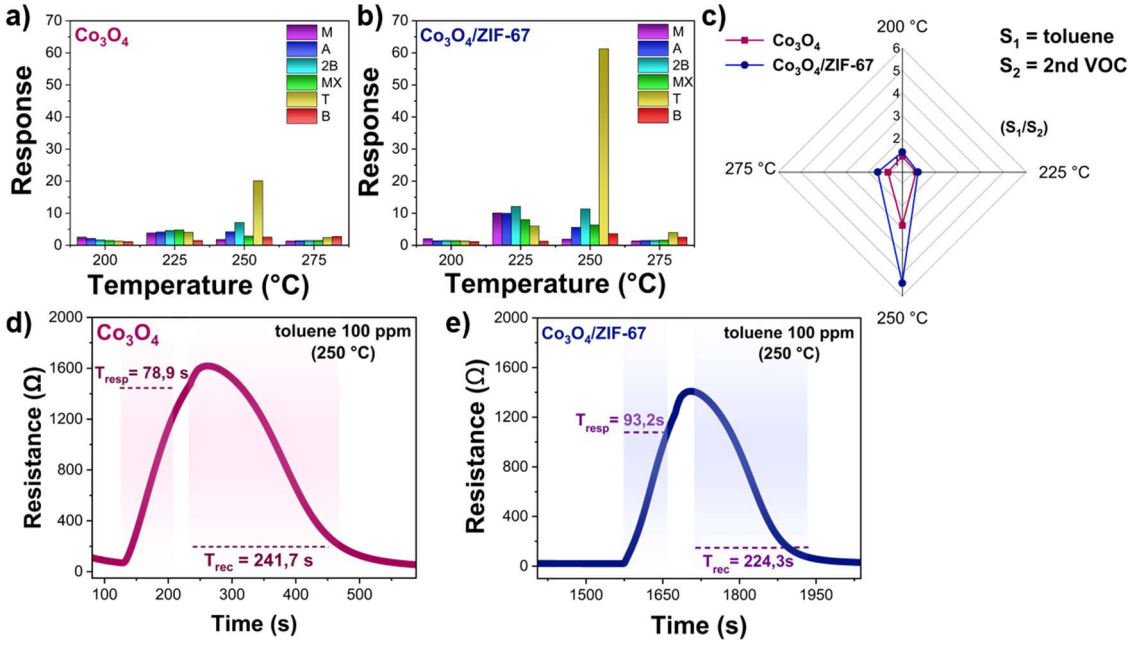


Source: Author

The gas detection capabilities of the $Co_3O_4$/ZIF-67 sensor were evaluated three times under the same conditions (100 ppm, 250 °C, and dry air) for six VOCs to calculate the sensor's average response, as shown in Fig. 8a. The $Co_3O_4$/ZIF-67 sensor exhibited a response of 55.6 ± 5.0. The repeatability assessment of the sensor for 100 ppm toluene is illustrated in Fig. 8b,c. The sensor displayed consistent and reproducible performance when detecting 100 ppm of toluene across 18 successive tests, yielding an average response of 47.6 ± 6.8 after the 18 application cycles under the abovementioned conditions. A declining response pattern was noted throughout the tests, suggesting that repeated applications affect the sensor. Fig. 8d illustrates the stability of the $Co_3O_4$/ZIF-67 sensor in measuring 100 ppm of toluene over 7 days at 250 °C in dry air, showing an average response of 72.4 ± 15.0.

The $Co_3O_4$/ZIF-67 sensor was exposed to a range of toluene concentrations, from 2 to 500 ppm, as shown in Fig.8e. As illustrated in Fig. 7e, an increase in toluene concentration results in a notable variation in the material's resistance, indicating a proportional rise in the sensor's response. In the concentration range of 2 to 500 ppm of toluene, the sensor exhibited a notable increase in response, from 1.3 to 85.6.

Fig.8f illustrates a polynomial fit of the response curve concerning varying concentrations of toluene in dry air. The graph shows the response values for different concentrations of toluene, which allows the figure out a polynomial function that describes the relationship between the sensor's responses and the different concentrations of toluene. Adjusting the polynomial function reveals a strong correlation between the response values and the toluene concentrations.

Fig.8g illustrates the impact of humidity on the sensor's responses. In the present study, 100 ppm toluene was employed at 250 °C, with humidity variations (0, 60, and 80%). As illustrated in the figure, there was a notable decline in the observed response, with a reduction of approximately 49% observed when transitioning from dry air to 60% RH. In contrast, at 80% RH, the response decreased by approximately 44% compared to dry air. The reduction in the sensor material's response can be attributed to the tendency of water molecules to adsorb on the surface in humid conditions, thereby occupying active sites within the material. As these active sites are indispensable for the adsorption and reaction of the target gas, the interaction of the target gas with the sensor surface is diminished when they are occupied by water molecules, consequently reducing the response (MALEPE et al., 2023). Conversely, it was observed that there was an increase of roughly 9% in the response from 60 to 80% RH, indicating that the sensor exhibited a counterintuitive trend of decay, with a slight increase in the sensor's response in environments with relative humidity between 60-80%.

The response and recovery times for the sensor were determined using 100 ppm toluene at 250 °C at different RH (60 and 80%). As illustrated in Fig.8h, the $Co_3O_4$/ZIF-67 sensor exhibited response times of 75.2 seconds at 60% RH and 91.8 seconds at 80% RH. These findings demonstrate that the response time increases with an elevated relative humidity, indicating a diminished response rate. Nevertheless, the response times remain shorter than those observed for the sensor in dry air ($T_{resp}$ = 93.2 s, as illustrated in Fig. 6e). Conversely, the recovery time exhibited a slight decrease, reaching 535.3 seconds at 60% RH and 465.2 seconds

at 80% RH. Compared to the recovery time in dry air (224.3 s), the recovery time increased approximately twofold when the relative humidity was 60% or 80%.

The semiconductor gas absorption model establishes a relationship between the gas response ($S_g$) and its concentration ($C_g$), which is defined by the following equation:

$$\log(S_g - 1) = \log\alpha + \beta \log C_g \quad (1)$$

The response order and the type of oxygen species adsorbed on the material are indicated by β values close to 0.5 (associated with $O^{2-}$) and 1 for the $O^-$ species (THEODORO et al., 2024). Equation 1 can be utilized to estimate the quantity of oxygen species adsorbed on the $Co_3O_4$/ZIF-67 sensor. The connection between the logarithm of the response ($S_g$) and the concentration ($C_g$) in 100 ppm toluene is illustrated in Fig.8i. At a temperature of 250 °C in dry air conditions, there exists a strong linear correlation ($R^2$ = 0.96) between log ($S_g$ - 1) and log ($C_g$). The fitted line (β) slope recorded a value of 1.129, which is comparable to 1. Consequently, it is inferred that the primary oxygen species adsorbed on the $Co_3O_4$/ZIF-67 surface is $O^-$.

**Figure. 8.** $Co_3O_4$/ZIF-67 performance measurements for toluene at 250 °C in (a) average response for VOCs; (b) sensor repeatability to 100 ppm; (c) gas response from sensor repeatability analysis; (d) sensor stability over 7 days; (e) sensor response for different concentrations (2 to 500 ppm); (f) polynomial fit curve of response versus concentrations; (g) response of the sensor at different humidities; (h) response time and recovery time curves for the sensor at different RH; (i) log ($S_g$ -1) in function of the sensor's log $C_g$.

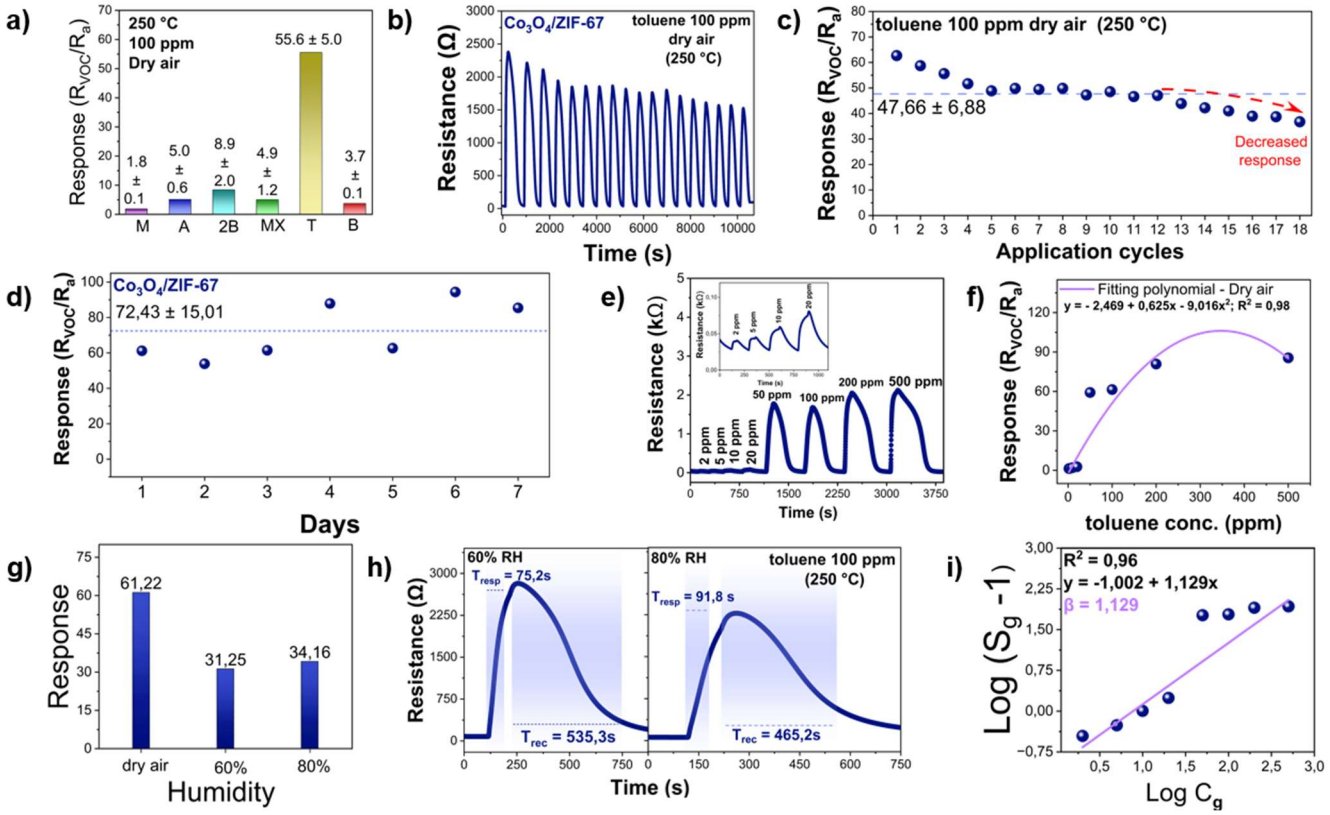


Source: Author

Table 2 illustrates the detection capabilities of the sensors synthesized in this study when compared with other sensors previously reported in the literature for the detection of volatile organic compounds (VOCs). The $Co_3O_4$/ZIF-67 sensor exhibited superior performance to the different sensors in the table, although it demonstrated higher response/recovery times compared to the other sensors presented in the table. These findings suggest using $Co_3O_4$/ZIF-67 for efficient detection of toluene.

**Table 2.** A comparison of toluene detection abilities in this study with those recorded in previous research.

| Sensor | Temperature (°C) | Concentration (ppm) | Response | Response time (s) | Recovery time (s) | Ref. |
|---|---|---|---|---|---|---|
| $Co_3O_4$ | 250 | 100 | 20.05 | 78.9 | 241.6 | This work |
| $Co_3O_4$/ZIF-67 | 250 | 100 | 61.22 | 93.2 | 224.3 | This work |
| $(C_3N_4)_{0.12}Co_3O_4$ | 220 | 100 | 17.02 | 104 | - | (NIU et al., 2023) |
| $Co_3O_4$ sheets | 180 | 200 | 8.5 | 10 | 30 | (ZHANG et al., 2020) |
| Hollow cubes of ZnO@$Co_3O_4$ | 290 | 100 | 26.4 | 11.2 | 12.5 | (SHI et al., 2023) |
| $In_2O_3$-ZnO | R.T* | 100 | 14.63 | 14 | 201 | (CAI; PARK; PARK, 2023) |

*R.T.: room temperature

Source: Author

## 2.4 Conclusion

This work presents the synthesis of $Co_3O_4$ micro-rods using the microwave-assisted hydrothermal method and the synthesis of the $Co_3O_4$/ZIF-67 composite using the reflux method. The findings demonstrate that the incorporation of ZIF-67 into the sensor material results in enhanced selectivity and a higher response for toluene. Our findings showed that the $Co_3O_4$ sensor exhibited a response of 20.0, while the $Co_3O_4$/ZIF-67 sensor demonstrated a response of 61.2. Consequently, the $Co_3O_4$/ZIF-67 sensor was deemed to be the superior of the two, exhibiting a selectivity index that was approximately twice that of the pure oxide sensor. The findings demonstrate that the $Co_3O_4$/ZIF-67 sensor exhibits enhanced toluene detection properties, including selectivity and sensitivity, which are superior to previously reported toluene sensors. Furthermore, the sensor demonstrated satisfactory performance in relatively humid environments. In conclusion, the $Co_3O_4$/ZIF-67 micrometric structure is a promising candidate for efficiently detecting toluene with minimal energy consumption.

## Acknowledgments

This study was financed in part by the Coordenação de Aperfeiçoamento de Pessoal de Nível Superior - Brasil (CAPES) – Finance Code 001. We also acknowledge the LSQA/IBILCE-UNESP laboratories for providing the XRD and FTIR techniques, LCE DEMa/UFSCar for TEM, and EDS data, LMA/IQ-UNESP for SEM. XAS analyses were performed at the IPE beamline at LNLS (SIRIUS – CNPEM, proposal – 20232482).

# 3 CONCLUSION AND NEXT CHALLENGES

The objective of this research was to develop $Co_3O_4$ sensors, in the presence and absence of ZIF-67, in order to examine the impact of incorporating a MOF into the sensor material on the detection of VOCs under diverse operational conditions. Chapter 2 presents a review of the principal topics, with a particular focus on VOCs and sensors based on semiconducting metal oxides (SMOs). The detection of volatile organic compounds (VOCs) is of paramount importance, given that these compounds are responsible for a few health issues affecting the general population, in addition to posing a significant environmental hazard. The synthesized $Co_3O_4$/ZIF-67 composite was found to be an excellent material for the detection of VOCs, particularly toluene. Chapter 3 outlines the synthesis of $Co_3O_4$ utilizing the microwave-assisted hydrothermal method, and the synthesis of $Co_3O_4$/ZIF-67 employing the reflux method. The incorporation of ZIF-67 resulted in enhanced sensor performance. At the optimal operating temperature, $Co_3O_4$/ZIF-67 exhibited heightened selectivity and superior toluene detection, although it demonstrated the longest response time. However, its recovery time was shorter in a dry environment.

Future challenges include the better characterization of the $Co_3O_4$/ZIF-67 sample using scanning electron microscopy (SEM) and transmission electron microscopy (TEM). This is necessary to obtain more detailed structural information on ZIF-67. This is because, of the characterization techniques carried out, it was only possible to identify the nitrogen present in the ZIF-67 ring using XAS. These analyses have contributed to a more nuanced understanding of the material's detection mechanism. Furthermore, this study seeks to facilitate future research into the advancement of *p*-type sensors through the incorporation of MOFs to enhance selectivity, while elucidating the impact of increasing porous materials, such as $Co_3O_4$/ZIF-67, on sensor performance, whether for toluene or other VOCs. Enhancing the selectivity and applications of sensors in authentic temperature and humidity conditions remains a significant challenge in this field.

# REFERENCES

BAGHERZADEH ENFERADI, S. M. H.; MIRZAEI, A. Fe2O3-Co3O4 nanocomposite gas sensor for ethanol sensing studies. **Ceramics International**, out. 2024.

BAI, G. et al. Porous Co3O4 nanowires and nanorods: Highly active catalysts for the combustion of toluene. **Applied Catalysis A: General**, v. 450, p. 42–49, jan. 2013.

CAI, G. et al. Template-Directed Growth of Well-Aligned MOF Arrays and Derived Self-Supporting Electrodes for Water Splitting. **Chem**, v. 2, n. 6, p. 791–802, jun. 2017.

CAI, Z.; PARK, J.; PARK, S. Porous In2O3–ZnO nanofiber-based sensor for ultrasensitive room-temperature detection of toluene gas under UV illumination. **Journal of Materials Research and Technology**, v. 24, p. 2482–2499, maio 2023.

CHEN, H. D. et al. High-valence cations-doped mesoporous nickel oxides nanowires: Nanocasting synthesis, microstructures and improved gas-sensing performance. **Sensors and Actuators B: Chemical**, v. 296, p. 126622, out. 2019.

CHEN, Y. et al. Trace detection of benzene, toluene and xylene (BTX) by chemiresistive metal oxide-based gas sensors: Recent advances in heterojunction materials design. **Chinese Chemical Letters**, p. 110606, nov. 2024.

CHO, S.-Y. et al. High-Resolution p-Type Metal Oxide Semiconductor Nanowire Array as an Ultrasensitive Sensor for Volatile Organic Compounds. **Nano Letters**, v. 16, n. 7, p. 4508–4515, 13 jul. 2016.

DEY, A. Semiconductor metal oxide gas sensors: A review. **Materials Science and Engineering: B**, v. 229, p. 206–217, mar. 2018.

DONG, M.; ZHANG, G.; MA, G. Co3O4@ZIF-67 core–shell heterogeneous catalyst for degradation of dye contaminants. **Inorganic Chemistry Communications**, v. 158, p. 111418, dez. 2023.

E.L. DA SILVA et al. **Microwave aided device for hydrothermal synthesis of nanostructured oxides, particularly obtaining particles of metal oxides, comprises container, in: Which Hydrothermal Reaction Takes Place, and Lid for Container.** , 2010.

FEI, Z. et al. Morphology-directed synthesis of $Co_3O_4$ nanotubes based on modified Kirkendall effect and its application in $CH_4$ combustion. **Chem. Commun.**, v. 48, n. 6, p. 853–855, 2012.

FENG, Y. et al. Strawberry-like Co3O4-Ag bifunctional catalyst for overall water splitting. **Applied Catalysis B: Environmental**, v. 299, p. 120658, dez. 2021.

HAJIVAND, P. et al. Application of metal-organic frameworks for sensing of VOCs and other volatile biomarkers. **Coordination Chemistry Reviews**, v. 501, p. 215558, fev. 2024.

HU, M. et al. Enhanced acetone sensing of MOFs derived Co3O4-ZIF hierarchical structure under the strategy of internal construction and external modification. **Sensors and Actuators B: Chemical**, v. 402, p. 134889, mar. 2024.

LEIDINGER, M. et al. Selective Detection of Hazardous Indoor VOCs Using Metal Oxide Gas Sensors. **Procedia Engineering**, v. 87, p. 1449–1452, 2014.

LETSHOLATHEBE, D. et al. Optical and structural stability of Co3O4 nanoparticles for photocatalytic applications. **Materials Today: Proceedings**, v. 36, p. 499–503, 2021.

LI, T. et al. The improved activity of Co3O4 nanorods using silver in the catalytic oxidation of toluene. **Environmental Science and Pollution Research**, v. 28, n. 28, p. 37592–37602, 14 jul. 2021.

LIU, H. et al. Construction of hollow NiO/ZnO p-n heterostructure for ultrahigh performance toluene gas sensor. **Materials Science in Semiconductor Processing**, v. 141, p. 106435, abr. 2022.

LIU, Y.; ZHANG, X.; WU, Y. Hydrothermal synthesis of Co3O4 with different morphologies and the improvement of lithium storage properties. **Materials Chemistry and Physics**, v. 128, n. 3, p. 475–482, 15 ago. 2011.

LOU, X. et al. Bimetallic zeolite imidazolate framework for enhanced lithium storage boosted by the redox participation of nitrogen atoms. **Science China Materials**, v. 61, n. 8, p. 1040–1048, 25 ago. 2018.

LUO, S. et al. Conductometric methane gas sensors based on ZnO/Pd@ZIF-8: Effect of dual filtering of ZIF-8 to increase the selectivity. **Sensors and Actuators B: Chemical**, v. 383, p. 133600, 15 maio 2023.

MAKHLOUF, S. A. et al. Structural, electrical and optical properties of Co3O4 nanoparticles. **Superlattices and Microstructures**, v. 64, p. 107–117, dez. 2013.

MALEPE, L. et al. A humidity-resistant and room temperature carbon soot@ZIF-67 composite sensor for acetone vapour detection. **Nanoscale Advances**, v. 5, n. 7, p. 1956–1969, 2023.

MARIAMMAL, R. N.; RAMACHANDRAN, K. Study on gas sensing mechanism in p-CuO/n-ZnO heterojunction sensor. **Materials Research Bulletin**, v. 100, p. 420–428, abr. 2018.

MIRZAEI, A.; LEONARDI, S. G.; NERI, G. Detection of hazardous volatile organic compounds (VOCs) by metal oxide nanostructures-based gas sensors: A review. **Ceramics International**, v. 42, n. 14, p. 15119–15141, nov. 2016a.

MIRZAEI, A.; LEONARDI, S. G.; NERI, G. Detection of hazardous volatile organic compounds (VOCs) by metal oxide nanostructures-based gas sensors: A review. **Ceramics International**, v. 42, n. 14, p. 15119–15141, nov. 2016b.

MOLHAVE, L. Volatile Organic Compounds, Indoor Air Quality and Health. **Indoor Air**, v. 1, n. 4, p. 357–376, dez. 1991.

NIU, J. Y. et al. Mesoporous Co3O4 nanowires decorated with g-C3N4 nanosheets for high performance toluene gas sensors based on p-n heterojunction. **Materials Chemistry and Physics**, v. 293, p. 126980, jan. 2023.

PERRONE, O. M. et al. Highly efficient detection of ethanol by SnO2 nanoparticles-decored NiO nanocuboids. **Materials Research Bulletin**, v. 158, p. 112086, fev. 2023.

QUANG, P. L. et al. Simple post-synthesis of mesoporous p-type Co3O4 nanochains for enhanced H2S gas sensing performance. **Sensors and Actuators B: Chemical**, v. 270, p. 158–166, out. 2018.

SAAD, R. et al. Highly sensitive and room-temperature operable carbon dioxide gas sensor based on spin-coated Sn-doped Co3O4 thin films with advanced recovery properties. **Surfaces and Interfaces**, v. 55, p. 105309, dez. 2024.

SABOURIN, P. J.; BECHTOLD, W. E.; HENDERSON, R. F. A high pressure liquid chromatographic method for the separation and quantitation of water-soluble radiolabeled benzene metabolites. **Analytical Biochemistry**, v. 170, n. 2, p. 316–327, maio 1988.

SHI, J. et al. Facile MOF-on-MOF isomeric strategy for ZnO@Co3O4 single-shelled hollow cubes with high toluene detection capability. **Applied Surface Science**, v. 609, p. 155271, jan. 2023.

THEODORO, R. DOS S. et al. Multiple-Yolk–Shell NiO Microspheres for Selective Detection of *m* -Xylene. **ACS Applied Materials & Interfaces**, 5 out. 2024.

THEODORO, R. S. et al. Tuning humidity for highly selective detection of methanol and 2-butanone using MOF-derivatives NiO microrods. **Journal of Materials Science: Materials in Electronics**, v. 34, n. 34, p. 2232, 1 dez. 2023.

VAN DEN BROEK, J. et al. Highly selective gas sensing enabled by filters. **Mater. Horiz.**, v. 8, n. 3, p. 661–684, 2021.

VESELY, P. et al. Analysis of Aldehydes in Beer Using Solid-Phase Microextraction with On-Fiber Derivatization and Gas Chromatography/Mass Spectrometry. **Journal of Agricultural and Food Chemistry**, v. 51, n. 24, p. 6941–6944, 1 nov. 2003.

WANG, C. et al. Metal Oxide Gas Sensors: Sensitivity and Influencing Factors. **Sensors**, v. 10, n. 3, p. 2088–2106, 15 mar. 2010.

WANG, L. et al. Highly improved toluene gas-sensing performance of mesoporous Co3O4 nanowires and physical mechanism. **Materials Research Bulletin**, v. 140, p. 111329, ago. 2021.

WANG, L. et al. Nanocasting synthesis and highly-improved toluene gas-sensing performance of Co3O4 nanowires with high-valence Sn-doping. **Chemical Physics**, v. 560, p. 111573, ago. 2022.

WANG, S. et al. MOF-derived Au functional CeO2/Co3O4 heterostructure gas sensor with moisture resistance for low-temperature and efficient toluene detection. **Journal of Alloys and Compounds**, v. 1010, p. 177358, jan. 2025.

WANG, W. et al. Detection of xylene from C/Co3O4 nanocomposites synthesized from double-template using g-C3N4/ZIF-67. **Chemical Engineering Journal**, v. 466, p. 143363, 15 jun. 2023.

WANG, X. X. et al. Nitrogen-Coordinated Single Cobalt Atom Catalysts for Oxygen Reduction in Proton Exchange Membrane Fuel Cells. **Advanced Materials**, v. 30, n. 11, 24 mar. 2018.

WEBER, I. C.; GÜNTNER, A. T. Catalytic filters for metal oxide gas sensors. **Sensors and Actuators B: Chemical**, v. 356, p. 131346, abr. 2022.

XIE, T. et al. High responsive n-butanol gas sensor based on MOFs-derived Cr2O3/RGO p-p heterojunctions materials. **Journal of Alloys and Compounds**, v. 1002, p. 175271, out. 2024.

XU, J. M.; CHENG, J. P. The advances of Co 3 O 4 as gas sensing materials: A review. **Journal of Alloys and Compounds**, v. 686, p. 753–768, nov. 2016.

YAN, Z. et al. Co 3 O 4 nanorod-supported Pt with enhanced performance for catalytic HCHO oxidation at room temperature. **Applied Surface Science**, v. 404, p. 426–434, maio 2017.

YAO, X. et al. Bimetallic MOF-derived CeO2/Co3O4 microflowers with synergy of oxygen vacancy and p-n heterojunction for high-performance n-butanol sensors. **Materials Today Communications**, v. 33, p. 104445, 1 dez. 2022.

YIN, X.-T. et al. Ultra-high selectivity of H2 over CO with a p-n nanojunction based gas sensors and its mechanism. **Sensors and Actuators B: Chemical**, v. 319, p. 128330, set. 2020.

ZHANG, R. et al. Facile preparation of hierarchical structure based on p-type Co3O4 as toluene detecting sensor. **Applied Surface Science**, v. 503, p. 144167, fev. 2020.

ZHANG, R. et al. Tracking the Role of Defect Types in $Co_3O_4$ Structural Evolution and Active Motifs during Oxygen Evolution Reaction. **Journal of the American Chemical Society**, v. 145, n. 4, p. 2271–2281, 1 fev. 2023.

ZHONG, J. et al. Toluene oxidation process and proper mechanism over Co3O4 nanotubes: Investigation through in-situ DRIFTS combined with PTR-TOF-MS and quasi in-situ XPS. **Chemical Engineering Journal**, v. 397, p. 125375, out. 2020.

ZITO, C. A. et al. Enhanced butanone chemoresistive sensor utilizing cobalt oxide nanoparticles. **Ceramics International**, v. 50, n. 15, p. 27147–27153, ago. 2024.